

Design of Novel Bainitic Steels: Moving from UltraFine to Nanoscale Structures

F.G. CABALLERO,^{1,3} C. GARCIA-MATEO,¹ and M.K. MILLER²

1.—National Center for Metallurgical Research (CENIM-CSIC), Avda Gregorio del Amo, 8, 28040 Madrid, Spain. 2.—Oak Ridge National Laboratory (ORNL), Oak Ridge, TN 37831-6139, USA. 3.—e-mail: fgc@cenim.csic.es

The concepts of phase transformation theory can be exploited to design nanostructured steels that transform to bainite at temperatures as low as 150°C. The microstructure obtained is so refined that it is possible to achieve strength in excess of 2.5 GPa in a material that has considerable toughness (40 MPam^{1/2}). Such a combination of properties has never been achieved before with bainite. A description of the characteristics and significance of this remarkable microstructure in the context of the mechanism of transformation is provided.

INTRODUCTION

There is a growing awareness of the potential benefits of nanoengineering in the modern steel industry, and leading research and development institutes and companies are pursuing research in the area of nanostructured steels. In this industry, the term “ultrafine grained” is generally used to describe steels with average grain sizes between 1 μm and 2 μm, and the term “submicron (submicrometer) structure” refers to grain sizes between 100 nm and 1000 nm. Until recently, effective processing techniques to reduce the grain size of these materials to less than 100 nm did not exist.

There are major difficulties in creating novel nanostructures that have a combination of properties appropriate for large-scale applications. An important requirement is to be able to manufacture large three-dimensional nanostructured components. In addition, the material concerned must be cost effective to produce, if it is not to be limited to niche applications. Severe deformation by methods such as mechanical milling, equal-channel angular processing, and high-pressure torsional straining has not succeeded in this respect. Although mechanical milling and alloying can produce powders containing nanosized grains, grain growth cannot effectively be suppressed during consolidation processes such as sintering and hot pressing. Therefore, processing bulk nanocrystalline materials for structural applications still poses a significant challenge, particularly in achieving an industrially viable process. Various processing

strategies and alloy developments currently being explored in the modern steel industry that have the potential for creating extremely strong and affordable nanostructured engineering steels have been recently reviewed elsewhere.¹

In the case of ferritic steels, it is possible to move from ultrafine to nanoscale by bainite reaction without the use of severe deformation, rapid heat treatment or mechanical processing. This new generation of steels has been designed in which transformation at low temperature leads to a nanoscale microstructure consisting of extremely fine, 20–40-nm-thick plates of ferrite and retained austenite.^{2–9} These microstructures are achieved through isothermal transformation to bainite of high-carbon, high-silicon steels with low martensite start temperature (~120°C). This process is similar to that applied to well-known commercial steels such as 100Cr6, for particular applications such as diesel injectors or large bearings.¹⁰ Nanostructured bainitic steels present the highest strength/toughness combinations ever recorded in bainitic steels (~2.5 GPa/40 MPam^{1/2})^{11,12} and exceptional rolling-sliding wear performances.^{13,14} The main objective of this article is to illustrate the characteristics and significance of this remarkable microstructure in the context of the mechanism of transformation.

LOW-TEMPERATURE BAINITE AND SLOW TRANSFORMATION KINETICS

In general, low transformation temperatures are associated with fine microstructures that in turn

generally possess both strength and toughness. There is, in principle, no lower limit to the temperature at which bainite can be generated according to bainite transformation theory.¹⁵ Thermodynamics calculations by Garcia-Mateo et al.³ and Caballero and Bhadeshia¹⁶ showed that it should be possible to obtain bainite at room temperature, but kinetics predicted that the transformation time would be approximately 100 years. An appropriate alloy was made 10 years ago to test this theory. Two samples were archived—one at Cambridge University and the other at the Science Museum in London. The samples are sealed in quartz tubes containing pure argon. The tubes will be broken in 100 years to determine whether bainite has formed and to conduct a detailed characterization. The samples were polished to a mirror finish so that any phase change will be evident in the mean time, through surface rumples caused by transformation.

The theoretical design procedure described elsewhere^{9,17} was used to produce, in a reasonable time, the finest possible bainitic structure by transformation at the lowest possible temperature.^{3,16} From the models, the so-called NANOBAIN steel compositions in Table I were defined to decrease bainite transformation temperature, increase the maximum volume fraction of bainite in the final microstructure, and improve the hardenability of the steels. The carbon concentration was selected from calculations to suppress the B_S temperature, with the aim of obtaining extremely thin platelets of bainite.

The bainite reaction in NANOBAIN 1 steel was found to take between 2 and some 90 days to complete the transformation within the temperature range 125–325°C,^{3,16} as illustrated in Fig. 1. Slow reactions give the ability to transform large components to a uniform microstructure free from residual stresses or complex processing. However, in a commercial scenario, there may be a need for more rapid heat treatment. Anything that enhances the nucleation rate will accelerate transformation, and the most

common way of doing this is by refining the austenite grain size. The number density of nucleation sites increases inversely with the austenite grain size. By deforming the austenite, which is often referred to as “pancaking” the austenite grains, the amount of austenite grain boundary area per unit volume may be further increased; the increase in grain surface area can be predicted quantitatively.¹⁸ If the austenite is left in the deformed state, then other defects such as shear bands and dislocations may also contribute to the nucleation rate. However, such defects can, in the case of displacive transformations, retard kinetics by a phenomenon known as mechanical stabilization.¹⁹

Another technique is to increase the magnitude of the free energy change accompanying the decomposition of austenite ($\Delta G^{\gamma\alpha} = G^\alpha - G^\gamma$), i.e., the

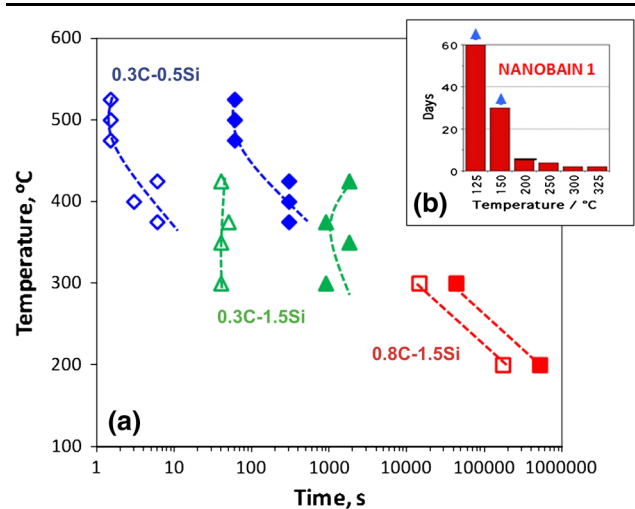


Fig. 1. (a) Kinetics results in terms of start and finish bainite reaction times as a function of transformation temperature in steels with different carbon and silicon contents with the approximated composition of Fe-XC-YSi-1.5Mn-0.5Cr (wt.%). (b) Histogram shows the required time (in days) to complete bainite reaction at different temperatures in the first generation of nanostructured bainitic steels (NANOBAIN 1 steel).

Table I. Chemical composition of nanostructured bainitic steels, wt.%

Steel	C	Si	Mn	Cr	Mo	V	Nb	Co	Al
First generation									
NANOBAIN 1	0.79	1.59	1.94	1.33	0.30	0.11	—	—	—
NANOBAIN 2	0.83	1.57	1.98	1.02	0.24	—	—	1.54	—
NANOBAIN 3	0.78	1.49	1.95	0.97	0.24	—	—	1.60	0.99
Second generation									
NANOBAIN 4	0.99	1.58	0.76	0.45	—	—	—	—	—
NANOBAIN 5	1.00	1.53	0.75	0.51	—	—	0.02	—	—
NANOBAIN 6	1.01	1.51	0.82	0.46	0.10	—	—	—	—
NANOBAIN 7	0.98	2.90	0.77	0.45	—	—	—	—	—
NANOBAIN 8	0.88	1.54	0.69	0.50	—	—	—	—	—
NANOBAIN 9	0.67	1.60	1.25	1.50	—	—	—	—	—
NANOBAIN 10	0.61	1.45	0.76	2.42	—	—	—	—	—
NANOBAIN 11	0.64	1.60	1.27	1.50	—	—	0.03	—	—
NANOBAIN 12	0.58	1.63	1.29	1.43	0.1	—	—	—	—

driving force for transformation, by making controlled additions of substitutional solutes to the steel. Both the nucleation and the growth rates can be expected to increase as a function of $|\Delta G^{yz}|$. The addition of cobalt and aluminum in the first generation of NANOBAIN (detailed compositions are given in Table I), boosts $|\Delta G^{yz}|$, causing the rate of transformation to increase.²⁰ The transformation was significantly accelerated to complete the processing within hours (as opposed to days) by making controlled additions of aluminum and cobalt in concentrations less than 2 wt.%. Another rate increment was possible in NANOBAIN 4–12 alloys (Table I) as kinetics data in Fig. 2 illustrate by reducing carbon, manganese, chromium, and molybdenum contents and by refining the prior austenite grain size with the help of niobium additions.^{9,14}

TENSILE PROPERTIES OF NANOSTRUCTURED BAINITIC STEELS

The bainite obtained by low-temperature transformation is harder than ever achieved for this

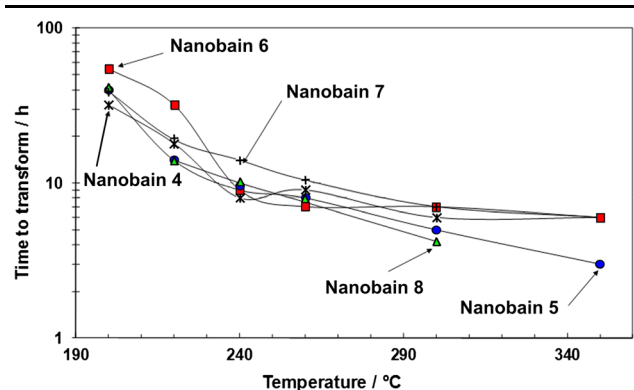


Fig. 2. Examples of the required time (in hours) to complete bainite reaction at different temperatures in the second generation of nanostructured bainitic steels.

microstructure, with values in excess of 700 HV. Some strength and ductility data at room temperature are illustrated in Fig. 3. The ultimate tensile strengths (UTS) were always in excess of 2 GPa, with non-negligible ductility. The detailed analysis of the results clearly outlines two groups: 0.6C grades (NANOBAIN 9–12) do not exhibit significant difference in tensile properties as a function of composition. However, for the same transformation temperature, higher carbon grades (1–0.8C, NANOBAIN 4–8) exhibit higher tensile strengths (typically 2200 MPa) and lower elongations, except for NANOBAIN 7. A particular surprise is the NANOBAIN 7 alloy, with extraordinary combination of ductility and strength, $\sim 12\%$ uniform elongation for UTS of 2 GPa.^{12,14}

Much of the strength and hardness of the structure comes from the incredibly thin platelets of bainitic ferrite.¹¹ For a true thickness t , the mean lineal intercept $\bar{L} \cong 2t$,²¹ the resulting strengthening is given by $\sigma \cong 115(\bar{L})^{-1}$ MPa where \bar{L} is in micrometers.^{22,23} The inverse dependence on \bar{L} , which does not follow the Hall–Petch relation, is because the transmission of slip across boundaries is determined by the energy required to expand dislocation loops rather than by the pile-up of the dislocations obstructed by boundaries.²³ The residue of strength after accounting for the plate thickness comes from dislocation forests, the intrinsic strength of the iron lattice, and solution strengthening.¹¹

In a similar scheme, attempts to understand the origin of ductility in most specimens have been met with only partial success. Indeed, the selected microstructural parameters (retained austenite or bainitic ferrite content and lath thickness) fail to provide any indication of the ductility; see some results in Table II, where similar parameters lead to significantly different ductility, with a clear difference in results when heat treating at 200°C/220°C or 250°C/270°C. As an example, NANOBAIN 7 exhibits identical retained austenite and bainite lath

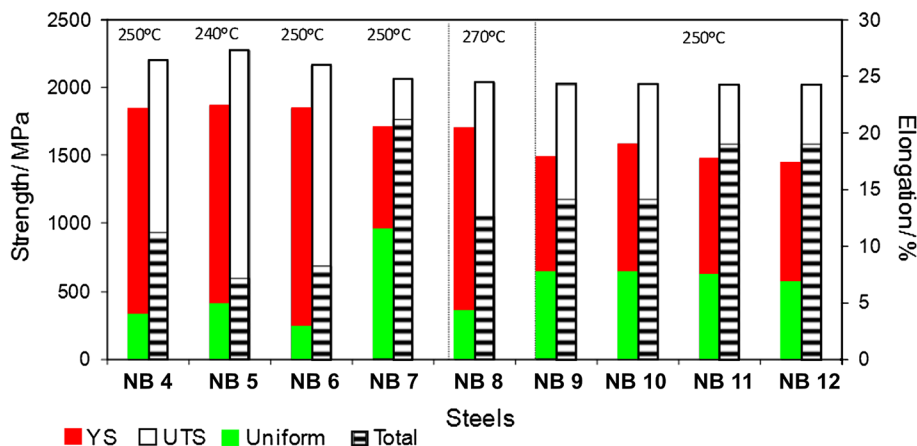


Fig. 3. Relevant tensile properties of second generation of nanostructured bainitic steels. NB is NANOBAIN. The temperature indicated refers to that of the isothermal transformation.

Table II. Tensile test and microstructural characterization results on selected grades and conditions

Alloy	T , °C	YS, MPa	UTS, MPa	UE, %	TE, %	V_γ , %	t , nm
NANOBAIN 6	200	2019	2091	0.37	0.38	20	21
	250	1852	2164	2.86	8.29	22	32
NANOBAIN 7	220	1704	2287	7.37	7.37	36	32
	250	1698	2068	11.62	21.32	34	32
NANOBAIN 8	220	1931	2329	3.19	4.1	22	32
	270	1701	2036	4.44	12.64	24	36

t bainitic ferrite plate thickness, T isothermal transformation temperature, TE total elongation, UE uniform elongation, UTS ultimate tensile strength, V_γ austenite volume fraction, YS yield strength.

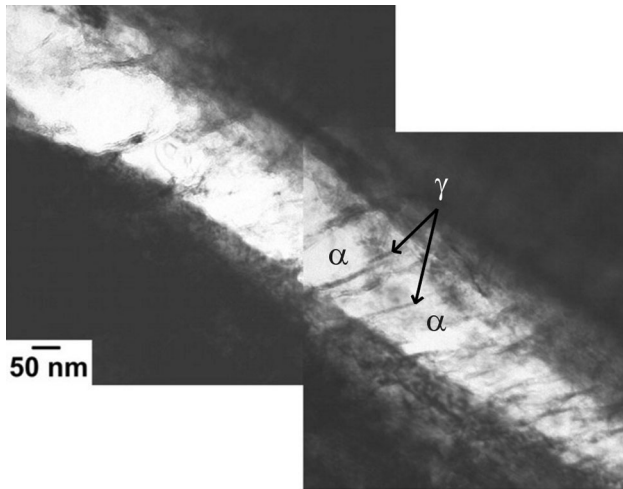


Fig. 4. Transmission electron micrographs of microstructure obtained at 125°C for 60 days in NANOBAIN 1 steel.

thickness after heat treatment at 220°C and 250°C, but its ductility is entirely different. It has been suggested that retained austenite mechanical stability is the key to the ductility in those microstructures.^{12,24}

NANOSCALE AND COMPLEX FERRITIC STRUCTURE

A bright-field transmission electron microscopy (TEM) image of NANOBAIN 1 steel transformed at 125°C for 60 days is presented in Fig. 4. Some of the plates of bainite are incredibly long and thin (20–40 nm), giving an ultrafine scale structure consisting of an intimate mixture of austenite and ferrite. Dislocation debris is evident in both the bainitic ferrite and the surrounding austenite. Extensive TEM failed to identify significant carbide precipitation in this low-temperature bainite; only a few extremely fine (20 nm wide and 175 nm long) cementite particles in the bainitic ferrite were found in samples after extensive aging at 200°C for 14 days.²

Ferrite laths in a bainite sheave are of nearly the same crystallographic orientation. The sheaves are sometimes called packets in optical microscopy,²⁵ as

they are similar to those of lath martensite. In lath martensite structures, a prior austenite grain is divided into packets, which are the group of laths with the same habit plane (or the same parallel close-packed planes relationship) with respect to austenite, and each packet is further divided into blocks.²⁶ Each martensite block contains laths of the same orientation and was called a co-variant packet.²⁷ Recently, the crystallography of bainite in Fe-9Ni-(0.15–0.5)C (wt.%) alloys transformed at different temperatures was studied in detail by electron backscatter diffraction (EBSD) in scanning electron microscopy (SEM).²⁸ It is known that the relative orientations of the bainitic ferrite and its parent austenite are always close to the classic Kurdjumov–Sachs (K–S) and Nishiyama–Wasserman (N–W) relationships.²⁵ From a single austenite grain, 24 crystallographic variants can be formed with a K–S orientation relationship and 12 with a N–W orientation relationship due to the symmetry of cubic systems. The inverse pole figure color map image in Fig. 5 shows the bainitic structure formed from an austenite grain at 250°C in the NANOBAIN 9 steel. The colors correspond to the crystallographic orientation normal to the observed plane, representing different crystallographic variants. The boundaries were drawn where the misorientation angle is greater than 10°. The corresponding pole figure shows some orientation scattering from the ideal N–W orientation relationship. The ideal N–W orientations of the 12 variants are rotated to coincide with the actual {011} pole figure of the measured transformed bainite (Fig. 5b). Then, each variant was accordingly identified on the orientation map (Fig. 5a). It is revealed that a prior austenite grain (Fig. 5c) was divided by packets consisting of three blocks of which the orientations are entirely different to each other. Each block contains a single variant of the bainitic lath.

MORPHOLOGY AND SIZE OF AUSTENITE

The refinement of the microstructure to the nanoscale is not exclusive of the bainitic ferrite, as retained austenite trapped between the slender plates of ferrite, nanofilms, as those shown in Figs. 4 and 6, also have a size < 100 nm. In the past,

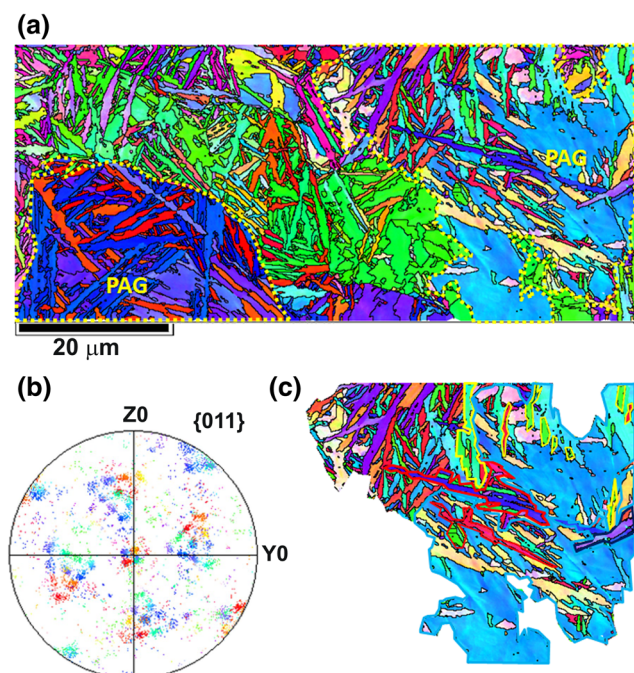


Fig. 5. (a) The inverse pole figure of NANOBAIN 9 transformed to bainite at 250°C. The black thin line represents the misorientation angles greater than 10° and the dashed yellow, coarse line represents selected prior austenite grain boundaries. (b) {011} Pole figure representing orientations of bainite laths corresponding to (a). (c) Enlarged prior austenite grain delimited in (a). The different coarse lines represent the packet boundaries.

the term block of austenite has been used to describe unetched surface pools of austenite with sizes of several tens of micrometers trapped between sheaves of bainite. In low-temperature bainitic alloys, the term microblock is used to denote blocks of retained austenite >1000 nm, and sub-micron blocks refers to those between 100 nm and 1000 nm.

Morphology is an important factor to be considered on the mechanical stability of austenite. In terms of its mechanical stability, thin films of retained austenite can be too stable^{29,30} to transform by transformation-induced plasticity (TRIP) effect for several reasons: first, because of the constraint to transformation exerted by the surrounding plates of ferrite; second, because smaller retained austenite contains lower potential nucleation sites for the transformation to martensite therefore requiring higher driving force for martensite nucleation; and finally, because of their higher carbon concentration.³¹

The chemical composition is an important factor controlling the mechanical stability of austenite. Elements such as carbon, manganese, and silicon^{32,33} significantly enhance the austenite mechanical stability; among these elements, carbon exhibits the strongest influence. In alloys containing austenite of low mechanical stability, the strain-induced transformation occurs during the early stages of deformation, resulting in little or no

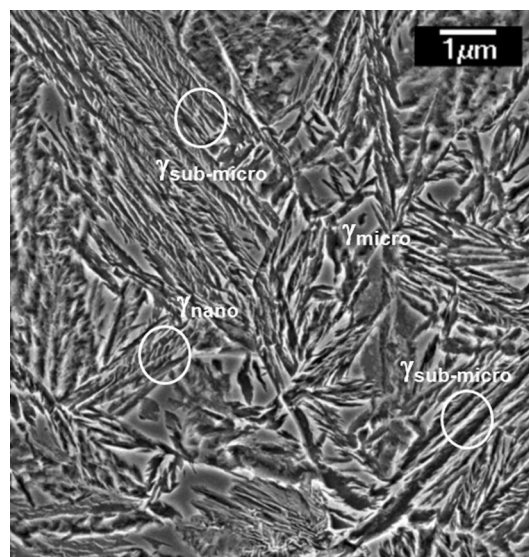


Fig. 6. Example of scanning electron micrograph of microstructures obtained in NANOBAIN 7 by isothermal transformation at 220°C.

benefit of the strain hardening related to deterring plastic instability or necking in the later stages of deformation. Conversely, if austenite becomes mechanically more stable and transforms at higher strains, then the associated strain hardening effectively increases resistance to necking and fracture. However, if austenite is too stable, then the presence of large amounts of austenite at necking (instability criterion) does not guarantee effective TRIP effect. So, the strain-induced transformation will enhance ductility if retained austenite is moderately stable against straining.

Therefore, a wide distribution of sizes of the retained austenite in the microstructure, as illustrated in Fig. 6, will lead to effective variations of the austenite stability and will be favorable for spreading the effect of the transformation all along straining and for postponing localization.^{34,35} As it has been mentioned and as Fig. 7 illustrates at an atomic level for these type of alloys,^{36,37} there is a strong correlation between the size of the austenite feature and the amount of C that is retained in solid solution; i.e., the smaller the size, the higher the amount of carbon present. Therefore, it can be concluded that a wider distribution of austenite sizes and a wider range of levels of mechanical stabilities might provide an extra contribution to ductility.¹²

HIGH DENSITY OF DEFECTS

Plastic relaxation in the austenite adjacent to the bainitic ferrite during bainite reaction may control the final size of the bainitic ferrite plates.³⁸ The defects generated in this process resist the advance of the bainitic ferrite–austenite interface, where the defect density is highest for lower transformation temperatures.³⁹ The plastic relaxation of the shape change was examined a long time ago by in situ

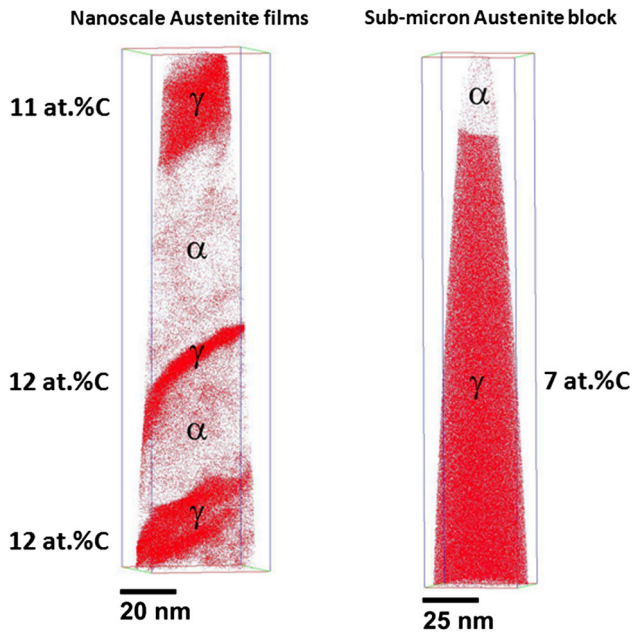


Fig. 7. Examples of carbon atom maps and corresponding carbon content for nanoscale films of austenite and submicron blocky austenite.

hot-stage TEM and prepolished samples of austenite transforming to bainite. Observations revealed that the growth of bainite is accompanied by the formation of dislocations in and around the bainite.⁴⁰

The retained austenite was also found to have the appearance of multiple planar faults/twins, often with one dominant fault plane.³¹ When the fault plane was approximately normal to the foil plane, the faults could be seen to terminate at slip steps in the austenite/ferrite interface indicative of accommodation slip on $\{111\}_\gamma$ planes during the displacive transformation.³¹

Cornide et al.⁴¹ determined the dislocation densities in the bainitic ferrite and austenite phases in nanostructured bainitic steels by TEM to be $(5.1 \pm 2.7) \times 10^{14} \text{ m}^{-2}$ and $(1.8 \pm 0.2) \times 10^{14} \text{ m}^{-2}$, respectively.⁴¹ These values are higher than those reported for conventional bainite, $1.7\text{--}4.0 \times 10^{14} \text{ m}^{-2}$ Ref. 42 and, in general terms, similar to those measured for martensitic microstructures.⁴³ A progressive increase in the dislocation density in bainitic ferrite was also observed as the austenite/bainitic ferrite interface is approached.⁴¹ This increase is related to the plastic deformation occurring in the surrounding austenite that accommodates the transformation strain as growth progresses and the following inheritance of those dislocations by the expansion of the growing bainitic ferrite plate.⁴¹

Complementary atom-probe tomography results revealed carbon trapping at dislocations in the vicinity of a bainitic ferrite-austenite interface, as shown in Fig. 8. The distribution of the carbon atoms in the analysis volume is not uniform, and carbon-rich and carbon-depleted regions are clearly

distinguishable. The carbon-enriched region at the top right of the atom map (Fig. 8b) represents austenite and the low carbon regions indicate the bainitic ferrite phase. Finally, the linear features with significant levels of carbon are dislocations in the vicinity of a bainitic ferrite-austenite interface. The 6 at.% C isoconcentration surface shown in Fig. 8b outlines the carbon-enriched region around a dislocation. It is evident from the proximity histograms across the dislocation in Fig. 8c that dislocations only trap the carbon atoms, as originally suggested by Kalish and Cohen.⁴⁴ As a result of the large distortion caused by the supersaturated carbon in the ferrite lattice, there is an attraction between carbon atoms and the stress fields of the dislocations.⁴⁵ Carbon tends to diffuse to sites close to dislocations to reduce its chemical potential.

NANOSCALE CARBIDES

The precipitation of carbides during the bainite reaction is a secondary process that is not essential to the mechanism of formation of bainitic ferrite, except where any precipitation influences the reaction rate by removing carbon either from the residual austenite or from the supersaturated ferrite.^{46,47} In upper bainite, the carbides precipitate from the carbon-enriched residual austenite between the developing laths. Thus, upper bainitic ferrite itself is generally free from intralath precipitates. In contrast, many observations reveal that lower bainitic cementite nucleates and grows within supersaturated bainitic ferrite in a process identical to the tempering of martensite.⁴⁸ The slower diffusion associated with the reduced transformation temperature provides an opportunity for some of the carbon to precipitate in the supersaturated bainitic ferrite. A fine dispersion of plate-like carbides is then found inside the bainitic ferrite, which also has a plate morphology, with a single crystallographic variant within a given bainitic ferrite plate, although it is possible to observe more than one variant of carbide precipitation in a lower bainite subunit.^{48,49}

Remarkably, the TEM micrograph shown in Fig. 4 failed to reveal carbide particles inside the bainitic ferrite after transformation at 125°C in NANOBAIN 1 steel, leading to the doubtful hypothesis that upper bainite was formed at this extremely low temperature. As mentioned above, only after extensive aging at 200°C for 14 days in the same steel, just a few 20 nm wide and 175 nm long cementite particles were observed by TEM inside a thicker bainitic ferrite plate.² The presence of intralath cementite as the lower bainite carbide in nanostructured bainitic steels was later confirmed by atom-probe tomography.⁵⁰ An example of a carbon atom map showing carbon segregation across a cementite particle in nanostructure bainitic steels is shown in Fig. 9. Cementite particles ideally contain a carbon content of 25 at.%; however, an apparent low carbon concentration of cementite was reported

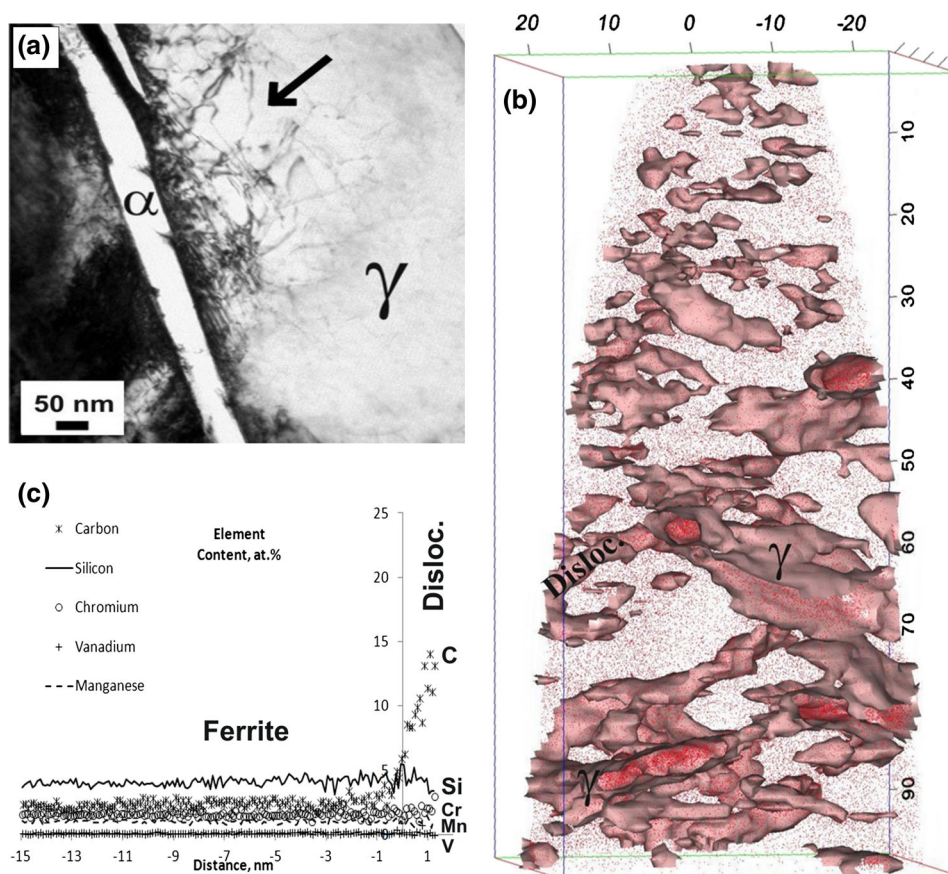


Fig. 8. (a) Transmission electron micrograph and corresponding (b) carbon isoconcentration surfaces at 6 at.% C. (c) Proximity histograms across a dislocation in ferrite in the vicinity of two austenite plates.

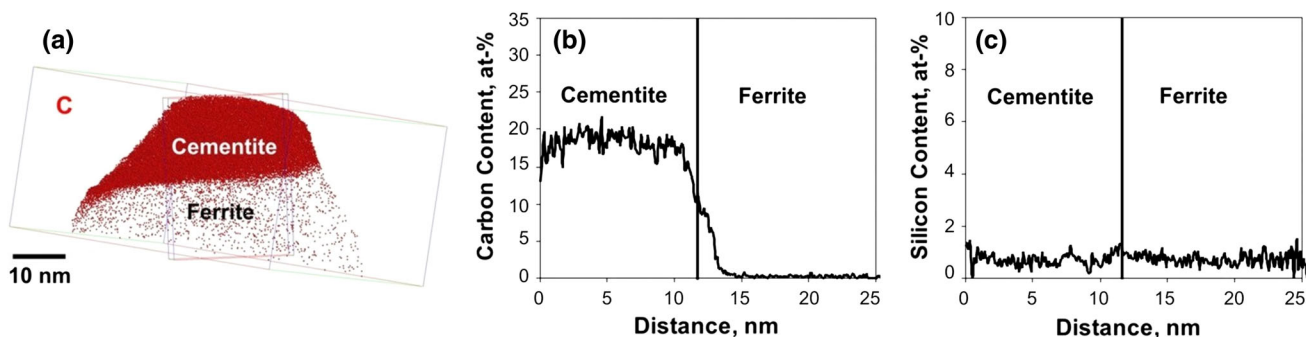


Fig. 9. (a) Carbon atom map and concentration profiles showing distribution of (b) carbon and (c) silicon across a cementite/ferrite interface during bainite transformation at 200°C in NANOBAIN 1.

in earlier atom-probe studies.^{51,52} This is primarily due to the assignment of the carbon peak at a mass-to-charge state ratio of 12 Da to be exclusively C^+ rather than containing some C_2^{++} ions, which will lead to a small underestimate of the true carbon level. However, all the particles detected with this level of carbon also show evidence of substitutional solute partitioning across the interface. The proximity histogram in Fig. 9 shows substitutional solute partitioning across the interface. This additional information helps to identify cementite.

As illustrated above, defects can effectively be thought of as separate trapping sites, which are a greater attractor for carbon than cementite. In these circumstances, the carbon available for cementite precipitation is reduced. The rate of precipitation then depends on the removal of defects during annealing, making more carbon available for cementite formation.⁵³ This process must greatly retard tempering kinetics and, because of the reduced carbon concentration in the perfect lattice, lead to a smaller driving force for precipitation.

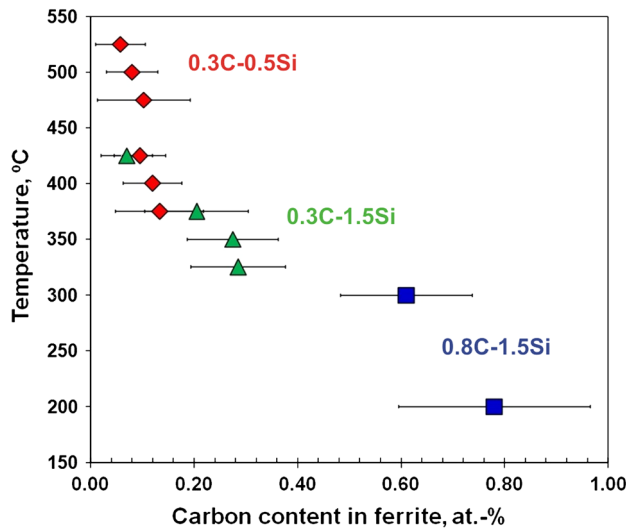


Fig. 10. Carbon content in bainitic ferrite determined by atom-probe tomography after bainite reaction at different temperatures in steels with the approximated composition of Fe-XC-YSi-1.5Mn-0.5Cr (wt.-%).

CARBON SUPERSATURATION IN FERRITE

In addition, atom-probe tomography revealed the presence of a high level of carbon in bainitic ferrite, which was well above that expected from para-equilibrium with austenite once the reaction proceeds to completion.⁵⁰ This reluctance of the carbon to partition was first attributed to the carbon trapping at dislocations in the vicinity of the austenite-ferrite interface and to the fact that the lower the reaction temperature, the higher dislocation density of bainitic ferrite. However, recent work⁵⁴ has also shown by atom-probe tomography (Fig. 10) that as the transformation temperature is decreased, a higher amount of carbon remains in defect-free solid solution in the bainitic ferrite after transformation. In fact, the recorded concentration profiles revealed that the carbon content is rather homogeneously distributed within each phase indicating that carbon had sufficient time to be distributed to a state close to certain kind of equilibrium that is independent of the initial distribution between bainitic ferrite and parent austenite.

An interesting question is what factors have caused the abnormally high carbon solubility in bainitic ferrite. Jang et al.⁵⁵ explained this abnormally high carbon content in ferrite using first-principles calculations and suggested that when tetragonal ferrite is in equilibrium with austenite, it has a much greater solubility for carbon than is the case for cubic ferrite in the same circumstances. Likewise, they provided experimental evidences for the existence of a tetragonal or slightly orthorhombic unit cell of bainitic ferrite that supports the hypothesis that the excess carbon that persists in the ferrite is a consequence of an increased solubility due to the change in symmetry from the conventional cubic unit cell.⁵⁶

SUMMARY

Nanostructured bainitic steels have been designed and manufactured following conventional industrial practices. Their microstructure consists of extremely fine plates of carbon-supersaturated ferrite and retained austenite. The designed steels present mechanical properties never achieved before with bainite, and the potential uses of these steels are many.

ACKNOWLEDGEMENTS

The authors gratefully acknowledge the support of the Spanish Ministry of Science and Innovation for funding this research under the contract MAT2010-15330, respectively. Atom-probe tomography research (M.K.M.) was supported through a user project supported by ORNL's Center for Nanophase Materials Sciences (CNMS), which is sponsored by the Scientific User Facilities Division, Office of Basic Energy Sciences, U.S. Department of Energy.

REFERENCES

1. F.G. Caballero and C. Capdevila, *Mater. Sci. Technol.* 29, 1149 (2013).
2. F.G. Caballero, H.K.D.H. Bhadeshia, K.J.A. Mawella, D.G. Jones, and P. Brown, *Mater. Sci. Technol.* 18, 279 (2002).
3. C. Garcia-Mateo, F.G. Caballero, and H.K.D.H. Bhadeshia, *ISIJ Int.* 43, 1238 (2003).
4. H.K.D.H. Bhadeshia, *Mater. Sci. Technol.* 21, 1293 (2005).
5. M. Soliman and H. Palkowski, *ISIJ Int.* 47, 1703 (2007).
6. P. Hodgson, I. Timokhina, X. Xiong, A. Yoshitaka, and H. Beladi, *Solid State Phenom.* 172-174, 123 (2011).
7. I.B. Timokhina, H. Beladi, X.Y. Xiong, Y. Adachi, and P.D. Hodgson, *Acta Mater.* 59, 5511 (2011).
8. J.A. Da Cruz Junior, T.F.M. Rodrigues, V.D.C. Viana, and D.B. Santos, *Mater. Sci. Forum* 706-709, 173 (2012).
9. C. Garcia-Mateo, T. Sourmail, F.G. Caballero, V. Smanio, M. Kuntz, C. Ziegler, A. Leiro, E. Vuorinen, R. Elvira, and T. Teeri, *Mater. Sci. Technol.* doi:10.1179/1743284713Y.0000000428.
10. ISO 683-17:1999, *Heat-Treated Steels, Alloy Steels and Free-Cutting Steels—Part 17: Ball and Roller Bearing Steels*, 1999.
11. C. Garcia-Mateo and F.G. Caballero, *ISIJ Int.* 45, 1736 (2005).
12. C. Garcia-Mateo, F. Caballero, T. Sourmail, M. Kuntz, J. Cornide, V. Smanio, and R. Elvira, *Mater. Sci. Eng. A* 549, 185 (2012).
13. A. Leiro, E. Vuorinen, K.G. Sundin, B. Prakash, T. Sourmail, V. Smanio, F.G. Caballero, C. Garcia-Mateo, and R. Elvira, *Wear* 298, 42 (2013).
14. T. Sourmail, F.G. Caballero, C. Garcia-Mateo, V. Smanio, C. Ziegler, M. Kuntz, R. Elvira, A. Leiro, E. Vuorinen, and T. Teeri, *Mater. Sci. Technol.* 29, 1166 (2013).
15. C. Garcia-Mateo and H.K.D.H. Bhadeshia, *Mater. Sci. Eng. A* 378, 289 (2004).
16. F.G. Caballero and H.K.D.H. Bhadeshia, *Curr. Opin. Solid State Mater. Sci.* 8, 251 (2004).
17. F.G. Caballero, M.K. Miller, C. Garcia-Mateo, C. Capdevila, and C. Garcia de Andrés, *JOM* 60 (12), 16 (2008).
18. Q. Zhu, C.M. Sellars, and H.K.D.H. Bhadeshia, *Mater. Sci. Technol.* 23, 757 (2007).
19. S. Chatterjee, H.S. Wang, J.R. Yang, and H.K.D.H. Bhadeshia, *Mater. Sci. Technol.* 22, 641 (2006).
20. C. Garcia-Mateo, F.G. Caballero, and H.K.D.H. Bhadeshia, *ISIJ Int.* 43, 1821 (2003).

21. H.K.D.H. Bhadeshia, *Mathematical Modelling of Weld Phenomena III* (London, U.K.: Institute of Materials, 1997), pp. 229–284.
22. G. Langford and M. Cohen, *ASM-Trans.* 62, 623 (1969).
23. G. Langford and M. Cohen, *Metall. Mater. Trans. A* 1, 1478 (1970).
24. C. Garcia-Mateo and F.G. Caballero, *Mater. Trans. JIM* 46, 1839 (2005).
25. H.K.D.H. Bhadeshia, *Bainite in Steels. Transformations, Microstructure and Properties*, 2nd ed. (London, U.K.: Institute of Materials, Minerals and Mining, 2001).
26. A.R. Marder and G. Krauss, *Trans. ASM* 60, 651 (1967).
27. S. Matsuda, T. Inoue, and M. Ogasawara, *Trans. JIM* 9, 343 (1968).
28. T. Furuhashi, H. Kawata, S. Morito, and T. Maki, *Mater. Sci. Eng. A* 431, 228 (2006).
29. C.A.N. Lanzillo and F.B. Pickering, *Met. Sci.* 16, 371 (1982).
30. N.K. Balliger and T. Gladman, *Met. Sci.* 15, 95 (1981).
31. H.K.D.H. Bhadeshia and D.V. Edmonds, *Metall. Trans. A* 10, 895 (1979).
32. P.J. Jacques, E. Girault, A. Mertens, B. Verlinden, J. Van Humbeeck, and F. Delannay, *ISIJ Int.* 41, 1068 (2001).
33. K. Nohara, Y. Ono, and N. Ohashi, *Tetsu-To-Hagane-J. ISIJ* 63, 212 (1977).
34. F. Lani, Q. Furnemont, T. Van Rompaey, F. Delannay, P.J. Jacques, and T. Pardoen, *Acta Mater.* 55, 3695 (2007).
35. K. Hase, C. Garcia-Mateo, and H.K.D.H. Bhadeshia, *Mater. Sci. Eng. A* 438–440, 145 (2006).
36. C. Garcia-Mateo, F.G. Caballero, M.K. Miller, and J.A. Jimenez, *J. Mater. Sci.* 47, 1004–1010 (2012).
37. F.G. Caballero, M.K. Miller, A.J. Clarke, and C. Garcia-Mateo, *Scr. Mater.* 63, 442 (2010).
38. L.C. Chang and H.K.D.H. Bhadeshia, *Mater. Sci. Technol.* 11, 105 (1995).
39. M.K. Fondekar, A.M. Rao, and A.K. Mallik, *Metall. Trans. A* 1, 885 (1970).
40. M. Nemoto, *High Voltage Electron Microscopy* (New York: Academic Press, 1974).
41. J. Cornide, G. Miyamoto, F.G. Caballero, T. Furuhashi, M.K. Miller, and C. Garcia-Mateo, *Solid State Phenom.* 172–174, 117 (2011).
42. G.M. Smith (Ph.D. Dissertation, University of Cambridge, 1984).
43. S. Morito, J. Nishikawa, and T. Maki, *ISIJ Int.* 43, 1475 (2003).
44. D. Kalish and M. Cohen, *Mater. Sci. Eng. A* 6, 156 (1970).
45. A.H. Cottrell and B.A. Bilby, *Proc. Phys. Soc.* 62A, 49 (1949).
46. H.K.D.H. Bhadeshia and J.W. Christian, *Metall. Trans. A* 21A, 767 (1990).
47. M. Takahashi and H.K.D.H. Bhadeshia, *Mater. Sci. Technol.* 6, 592 (1990).
48. H.K.D.H. Bhadeshia, *Acta Metall.* 28, 1103 (1980).
49. L.C. Chang, *Mater. Sci. Eng. A* 368, 175 (2004).
50. F.G. Caballero, M.K. Miller, S.S. Babu, and C. Garcia-Mateo, *Acta Mater.* 55, 381 (2007).
51. M.K. Miller, P.A. Beaven, S.S. Brenner, and G.D.W. Smith, *Metall. Trans. A* 14A, 1021 (1983).
52. S.S. Babu, K. Hono, and T. Sakurai, *Metall. Mater. Trans. B* 25, 499 (1994).
53. T.D. Bigg, D.K. Matlock, J.G. Speer, and D.V. Edmonds, *Solid State Phenom.* 172–174, 827 (2011).
54. F.G. Caballero, M.K. Miller, and C. Garcia-Mateo, *Acta Mater.* 58, 2338 (2010).
55. J.H. Jang, H.K.D.H. Bhadeshia, and D.-W. Suh, *Scr. Mater.* 68, 195 (2013).
56. C.N. Hulme-Smith, I. Lonardelli, A.C. Dippel, and H.K.D.H. Bhadeshia, *Scr. Mater.* 69, 409 (2013).